Soils and Rocks
www.soilsandrocks.com
An International Journal of Geotechnical and Geoenvironmental Engineering
ISSN 1980-9743
ISSN-e 2675-5475

Finite element analysis of soil-nailed vertical excavation in fine-grained soils in an urban area

Daniel Rocha Lanzieri[1], José Orlando Avesani Neto[1#]

Case Study

Keywords
Retaining wall
Finite element method (FEM)
Horizontal displacement
Nail tensile load
Nail pullout strength
Tensile load at nail head

Abstract

This paper presents analysis and discussion of an urban vertical excavation, with the soil nailing technique, in fine-grained soils with high plasticity. The excavation was numerically evaluated using finite element analysis (FEA) using a 3D finite element model (FEM). Several field and laboratory soil investigations were conducted, interpreted and used in the FEA. The FEM model was calibrated using instrumentation and monitoring results during the soil nailing construction. Analyses were conducted focusing in horizontal displacements, nail pullout strength, nail tensile load, soil stress state, and tensile load at the nail head. The results showed that the behavior of the soil nailing retaining wall in fine-grained soils differs significantly from what is typically reported in the literature for non-cohesive soils. The high apparent cohesion of the fine-grained soil resulted in good performance, with reduced horizontal displacements on the face and lower tensile loads in the nails and at their head.

1. Introduction

Since its initial use in the 1960s, the soil stabilization technique known as soil nailing, which involves the inclusion of passive steel bars in the soil mass, has gained popularity worldwide. This can be attributed to various factors, including the increasing need for stabilization in infrastructure and real estate projects, as well as excavations in urban areas. Additionally, soil nailing offers several technical advantages, such as feasibility, flexibility, ease of adjust in the field, rapid implementation, cost-effectiveness, and applicability to a wide range of soil types (Goyal & Shrivastava, 2022; Yadegari et al., 2023).

Despite the numerous advantages, there are still concerns raised by international guidelines regarding the use of soil nails in fine-grained soils. For instance, the FHWA Design Manual, also known as GEC7, does not recommend the use of soil nails in soils with a plasticity index (*PI*) greater than 20 (Bi et al., 2023; Lazarte et al., 2015; Sanchez et al., 2017).

Soil nailing has been successfully used for many years in clayey materials. In Brazil, soil nailing in clayey soils has been employed since the early of the 1970s, with thousands of projects already completed (Arêdes et al., 2020; Delmondes Filho et al., 2022; Ortigão et al., 1995; Porto et al., 2017). There are also records of soil nailing being used in clay materials in various other locations, including Germany, France, and Ireland in Europe (Cartier & Gigan, 1983; Juran & Elias, 1987; Menkiti & Long, 2008; Ostermayer, 1975), Australia (Poon et al., 2019), Asia (Babu et al., 2007; Bi et al., 2023) and the United States (Kamath, 2016; Mun & Oh, 2017; Oral & Sheahan, 1998; Turner & Jensen, 2005). Recently, Yuan et al. (2019) compiled information on approximately 40 soil nailing projects on clay soils in China, with heights ranging from 4 to 20 meters.

Soil nailing in fine-grained soils offers several advantages, including high-depth excavation self-support, reduction of lateral earth pressure, reduction of tensile stress in the nails due to cohesion and a setup effect similar to that of piles, which is a time-dependent increase in pile capacity (Briaud et al., 1998a, b). However, there are certain aspects that require attention when considering soil nailing in clayey soils, such as creep, and soil wetting and expansion (Papagiannakis et al., 2016; Poon et al., 2019; Sanchez et al., 2017).

In recent years, significant advancements have been made in the computational analysis of soil nailing in clayey soils. Numerous 2D and 3D models have been used to: analyze stresses and strains, investigate pullout behavior, and evaluate safety and effects of soil wetting and creep. These analyses have involved the use of various case studies and innovative techniques to simulate the soil-nail interaction (Barbosa et al., 2023; Briaud & Lim, 1997; Mun & Oh, 2017; Oliaei et al., 2019; Papagiannakis et al., 2016; Sanchez et al., 2017 Singh & Sivakumar Babu, 2010; Su et al., 2008; Taib & Craig, 2006; Ye et al., 2017; Zolqadr et al., 2016).

[#]Corresponding author. E-mail address: avesani@usp.br
[1]Universidade de São Paulo, Escola Politécnica, Departamento de Engenharia Estrutural e Geotecnia, São Paulo, SP, Brasil.
Submitted on October 25, 2023; Final Acceptance September 12, 2024; Discussion open until May 31, 2025.
Editor: Renato P. Cunha
https://doi.org/10.28927/SR.2025.010523

This article contributes to the this field by presenting a computational simulation of a vertical urban excavation supported by soil nailing in a clayey soil with high plasticity. The numerical model was calibrated using data obtained from a real work with instrumentation and monitoring during the construction process. The objective of the study was to further analyze the performance of soil nailing in fine-grained soils and improv the understanding of its effectiveness in such conditions.

2. Vertical excavation in an urban area

The soil nailing excavation was conducted as part of the expansion project for the Beneficencia Portuguesa Hospital in São Paulo city, Brazil. The excavation consisted of eight walls with a total area of 2,900 m^2 and depths ranging from 10 to 14 m. A total of 2,841 m^2 of soil nailing face was executed (Décourt et al., 2003). The excavation site was surrounded by nearby buildings. Figure 1A provides a plan view of the entire excavation area, highlighting the region of interest that was modeled in this study and Figure 1B depicts the three-dimensional model used in the analysis, representing the soil mass after excavation.

2.1 Walls modeled

The region of interest modeled includes Walls 2 and 6, as shown in Figure 1. Wall 6 was considered in the computational model to implement a 3D condition. However, the analyses were conducted using results from the field instrumentation of Wall 2.

Wall 2 had a length of 33.6 m and a height of 11.5 m. The excavation was performed vertically and required a total of 233 nails, each measuring 10 m in length. The nails were installed with a 10° inclination with the horizontal. The horizontal spacing between the nails was 1.30 m, while the vertical spacing was 1.35 m. Only the top row of nails had a reduced horizontal spacing of 0.65 m to minimize displacements on the surface. Similarly, Wall 6 had a length of 27.5 m and a height of 10.5 m. The geometric conditions for Wall 6 were the same as those for Wall 2, and a total of 180 nails were used.

The nails were installed using 75 mm diameter holes and 20 mm (3/4") steel rebars. Grout injection was performed in phases, with a water-cement ratio (*w/c*) of 0.5. The wall facing was constructed using 80 mm thick shotcrete reinforced with metallic fibers, with a steel rate of 40 kg/m^3. The nail-facing connection was achieved with 200 mm "L" bends on the steel bars, embedded in the shotcrete. Figure 2 provides additional geometric characteristics of the soil nail excavation.

2.2 Geotechnical investigation

A comprehensive site investigation campaign was conducted, which included several in situ and laboratory experiments. Standard penetration tests with torque measurement, cross-hole tests, and Camkometer pressiometer tests (Fioravante et al., 1994) were conducted to investigate the soil conditions. In addition, laboratory tests were conducted to complete the soil characterization.

The local subsoil consists of two main layers. The upper layer is a 7.5-m-thick surficial layer of silty-sandy porous clay, red in color and has a soft to medium consistency. This layer is referred to as "lateritic porous red clay". Below this layer, there is another silty-sandy clay layer that is yellow and gray in color. This bottom layer has a medium to stiff consistency and extends to a depth of more than 20 meters. It is known as "stiff clay". The water table was detected

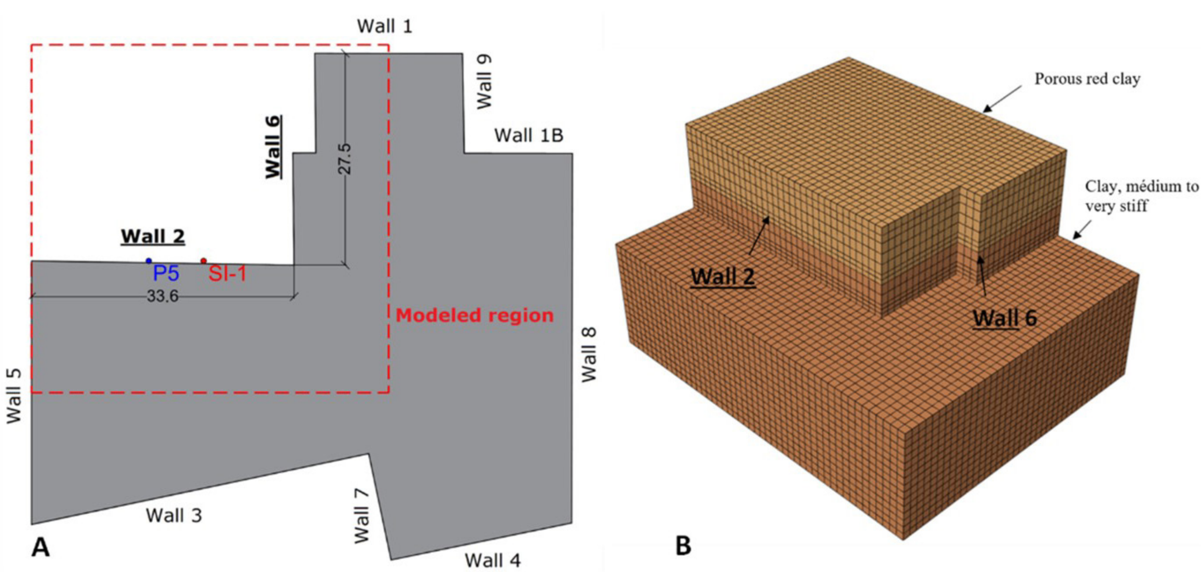

Figure 1. A. Excavation plan view with location of the modeled region and horizontal and vertical displacement instruments (dimensions in meters). B. 3D model used in FEM. P5: vertical displacement monitoring point. SI-1: inclinometer SI-1.

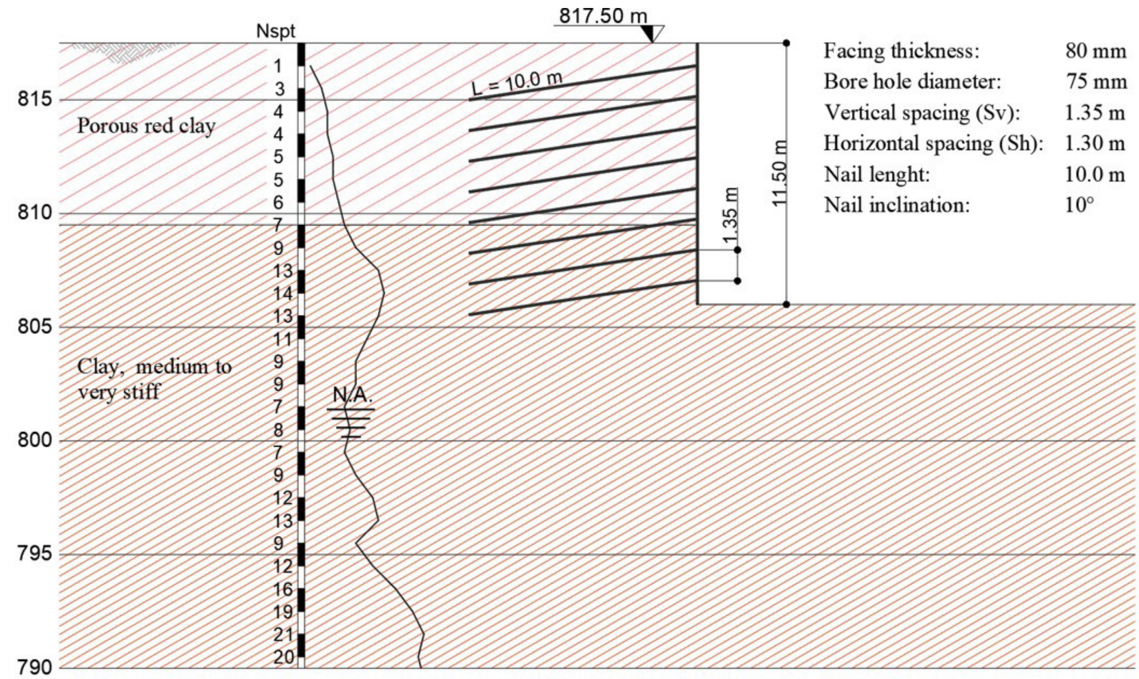

Figure 2. Schematic cross section of the excavation with characteristics of the subsoil and soil nailing.

at a depth of 16 meters. Figure 2 provides a geological-geotechnical profile that represents the region where Walls 2 and 6 are located.

The porous red clay is a typical lateritic tropical soil with a high fines fraction, comprising approximately 90% of the soil composition. The liquid limit (*LL*) of the soil was determined to be 84%, while the plasticity index (*PI*) was calculated as 41%. According to the Unified Soil Classification System (ASTM International, 2000), this soil can be classified as silt with high plasticity (*MH*). Additionally, based on the AASHTO soil classification system (Hogentogler & Terzaghi, 1929), the soil falls under the A.7.5 category.

The stiff clay, which is also a typical lateritic tropical soil, has fines fraction of more than 70%. The *LL* and *PI* were determined to be 78% and 35%, respectively. According to the USCS, the soil can also be classified as *MH*. The soil is also classified as A.7.5 by the AASHTO system.

2.3 Instrumentation and monitoring

The excavation was monitored throughout its perimeter using building and surface settlement marks, as well as inclinometers. This monitoring began in November 2002 and continued until the completion of the excavation in February 2003.

For the purposes of this paper, only the results from the instruments placed on Wall 2 are discussed. These instruments include ground settlement marks labeled as “P-5” located on the top of Wall 2, just 1.0 meter away from the face, and an inclinometer labeled as “SI-1” positioned on the back side of the wall. The location of these instrument elements can be seen in Figure 1.

3. Soil–nailed wall computational simulation

3.1 Finite element modelling

The behavior of Walls 2 and 6 was analyzed using numerical modeling with a FEM software. A 3D model was created using the Abaqus software and the analysis employed the Mohr Coulomb constitutive model. All the excavation steps were simulated, following the sequence of the construction process. The height of each excavation step was set to match the vertical spacing of the soil nails, with one line being executed at a time.

The soil mass was represented in the model using hexahedral solid elements known as C3D20R. These elements are three-dimensional and have 20 nodes used to simulate the behavior of the soil.

The soil nailing face was modeled as a “skin” with a thickness of 80 mm. This face was represented using flat elements, specifically the S8R element. The S8R element is a shell element with 8 nodes and reduced integration.

The nails were represented in the model using hexahedral elements called C3D20R. These elements are three-dimensional and have 20 nodes used to simulate the behavior of the nails.

The interface between the soil and the nail was modeled using a layer consisting of solid elements that were 4 mm thick. This technique has been previously used in several research to control the lateral friction between the soil and the nail in 3D models (Su et al., 2010; Zhou et al., 2013).

A quadratic interpolation function was employed for all elements, including solids and shells, with a reduction in the number of integration points. This choice of interpolation function was made considering factors such as processing time and the elimination of undesired phenomena during the analysis, such as “Hourglassing” (spurious energy deformation modes) and “shear locking”, which can lead to an increase in element stiffness during bending.

In terms of boundary conditions, horizontal displacements were restricted on the external sides of the model, allowing only vertical displacements. At the bottom of the model, both vertical and horizontal displacements were restricted.

3.2 Soil layers, nails, and soil–nail interfaces properties

Table 1 presents the materials parameters used in the FEA based on the in situ and laboratory tests conducted.

The strength parameters of the soils were established based on conducted triaxial compression tests, taking into account the range of stresses experienced at various depths during the excavation. This resulted in effective cohesions (c') of 20 and 25 kPa, and effective friction angles (ϕ') of 23° for the porous red clay and stiff clay, respectively, as shown in Table 1. These values fall within the ranges recommended by the technical standards of the São Paulo Subway Company and are consistent with findings from various articles on experiments and urban excavations in the region, considering the characteristics of the well-known soil (Décourt et al., 2003; Massad, 2012; Portelinha et al., 2023; São Paulo Metro, 1980).

The deformability parameters of the soils were determined using resonant column and cross-hole tests conducted within the range of excavation depths. The cross-hole tests revealed an increase in the initial shear modulus (G_0) with depth for the stiff clay, and this condition was considered in the analyses, as indicated in Table 1. Since the elastic parameters obtained from these tests are representative of low strain magnitudes, a correction was applied to consider the Young’s modulus within a strain range of 0.01 to 0.1% (Santos & Correia, 2001). These strain values are typical for retaining walls in excavation situations (Look, 2007).

The parameters and characteristics used for the shotcrete facing and the nails are also presented in Table 1. They were adopted based on the specific conditions of the soil nailing work and in accordance with the academic literature (Banthia et al., 2011; Malmgren, 2007; Singh & Sivakumar Babu, 2010; Suksawang et al., 2018).

4. Results and discussion

4.1 Horizontal displacements

Figure 3 compares the maximum horizontal displacement (δh) registered in the field for the last excavation phase (11.5 m) in this study with other soil nailing excavations

Table 1. Materials properties used in FEA.

	Porous red clay	Stiff clay
Unit weight, γ (kN/m^3)	15	17
Cohesion, c' (kPa)	20	25
Angle of internal friction, ϕ' (°)	23	23
Young modulus, E (MPa)	30	136+8z [1]
Poisson’s ratio, v	0.30	0.30
	Shotcrete facing	
Shotcrete thickness, d (mm)	80	
Unit weight, γ (kN/m^3)	25	
Young modulus, E (MPa)	20.000	
Axial stiffness, EA (kN)	1.6 x 10^6	
Bending stiffness, EI (kN.m^2/m)	853	
Poisson’s ratio, v	0.20	
	Nails	
Grouted diameter, $Ø$ (mm)	75	
Unit weight, γ (kN/m^3)	25	
Lenght, L (m)	10	
Young modulus, E (MPa)	200.000	
Axial stiffness, EA (kN)	8.8 x 10^6	
Bending stiffness, EI (kN.m^2/m)	31	
Poisson’s ratio, v	0.30	

[1]: Young modulus increasing with depth (z).

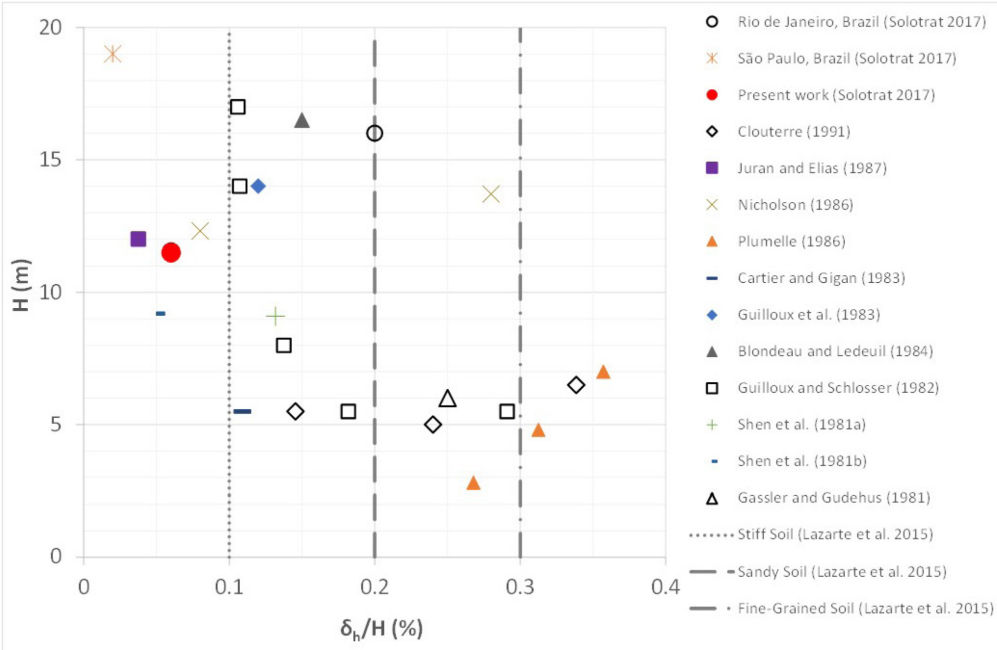

Figure 3. Comparison of the maximum horizontal displacements of soil nailing excavations.

conducted in Brazil and reported in the international literature. The comparison includes several conditions of retaining wall height, soil types and nails characteristics (Blondeau & Ledeuil, 1984; Cartier & Gigan, 1983; Clouterre, 1991; Gassler & Gudehus, 1981; Guilloux et al., 1983; Guilloux & Schlosser, 1982; Juran & Elias, 1987; Lazarte et al., 2015; Nicholson, 1986; Plumelle, 1986; Shen et al., 1981a, b; Solotrat, 2017).

The maximum horizontal displacement of 6.9 mm measured in the SI-1 inclinometer in this study, which corresponds to a horizontal deformation of 0.06% (0.6/1,000), is relatively low for soil nailing excavations, particularly in fine-grained soils. As summarized in Figure 3, soil nailing retaining walls typically exhibit a horizontal deformation ranging from 0.1% to 0.3%, depending on the soil type. According to FHWA's GEC7 (Lazarte et al., 2015), the expected value for horizontal deformation in clayey soils would be around 0.3%, which is significantly higher than the value observed in this study. Interestingly, as shown in the same figure, the present study achieved a condition very similar to that reported by another soil nailing retaining wall in a similar type of soil (Juran & Elias, 1987).

In the present study, the reduced horizontal deformation observed in the inclinometer measurements can be attributed to the high apparent cohesion of the unsaturated material. The presence of suction in the soil contributes to a higher cohesion value, which in turn reduces the lateral earth pressure and minimizes horizontal displacements and loading in the nails. As long as this unsaturated condition is maintained and an adequate drainage system is in place, the performance of the retaining wall remains high. The chart in Figure 3 also highlights another study conducted in São Paulo city, on a similar soil, which further supports the observation that horizontal displacements are indeed reduced under these conditions (Solotrat, 2017).

4.2 Nail pullout strength

Several nail pullout tests were conducted on-site using different cement grout injection conditions. These conditions included: i) filling the hole only, ii) filling the hole and applying pressure injection after 12 hours, and iii) filling the hole and applying two injection phases, each after 12 hours. The ultimate pullout strengths obtained from these tests ranged between 25 and 36 kN/m for all three conditions. The condition employed during the soil nailing execution was filling the hole and applying one injection phase (Décourt et al., 2003).

Figure 4 illustrates the pullout behavior obtained from the FEA. Unfortunately, no pullout strength versus pullout displacement charts were generated from the tests conducted on-site for comparing with the FEA results. However, the range of pullout strength values obtained from the field tests, as mentioned in the previous paragraph, is included in the same figure to facilitate a comparison between the results.

The behavior of the nail pullout resistance mechanism observed in the FEA model exhibits a peak resistance followed by a reduction in resistance after reaching the peak. This behavior, along with the magnitude of the ultimate pullout force and observed displacements, falls within the range reported in the international literature (Babu & Singh, 2010;

Clouterre, 1991; Oliaei et al., 2019; Pradhan et al., 2006; Zhu et al., 2010) and from tests conducted on Brazilian tropical soils (Décourt et al., 2003; Ehrlich & Silva, 2015; Silva, 2009; Solotrat, 2017). Additionally, the ultimate pullout strength obtained in the FEA model falls within the range of pullout strength values obtained from the field tests, as highlighted in Figure 4.

The parameters provided in Table 1 allow calculating the skin friction (q_s) values obtained from the FEA and those determined experimentally in the field by the pullout tests. For a hole with diameter of 75 mm, a skin friction value of 127 kPa was calculated from the FEA results, while a range of 106 to 153 kPa was recorded in the field tests. These values fall within the range typically reported in the literature for field and laboratory pullout tests on clayey soils (Bustamante & Doix, 1985; Clouterre, 1991). In Brazil, it is common practice to use skin friction correlations with the number of blows in the standard penetration test (*Nspt*) based on semi-empirical analysis and field tests for calculating pile bearing capacity (Barbosa et al., 2022; Ortigão, 1997; Ortigão et al., 1997). By using the q_s values obtained from the field pullout tests, which cover the range of results from the FEA, and retro-analyzing the two correlations mentioned, a range of *Nspt* values from 7 to 15 is obtained. These values closely align with the actual values recorded in the in-situ investigation, demonstrating the good predictive capacity.

4.3 Nail tensile load

Figure 5 shows the tensile loads, bending moments, and shear force in the nails obtained using the FEM after the final excavation step at a depth of 11.5 m. The figure also includes a line that connects the points of maximum nail tensile force along the retaining wall depth. Table 2 complements the results shown in Figure 5 by indicating the magnitude of the maximum nail tensile load (T_{max}) in each row, as well as the loads obtained at the nail head (T_0).

Based on the FEA results, as shown in Figure 5 and Table 2, it is evident that the maximum tensile forces are higher in the nails located closer to the bottom of the excavation and lower at the top. This phenomenon can be attributed to three factors. Firstly, greater depths result in higher vertical and horizontal stresses, leading to increased loads in the nails. Secondly, the first row of nails has twice as many reinforcements, resulting in lower loads in the reinforcements. Lastly, the portion of soil resistance due to apparent cohesion is significant for shallow depths, causing the lateral soil pressure in the upper portion of the excavation to be of low magnitude, thereby reducing the tensile loads in the nails in that region.

The highest value of tensile loads in the nails was calculated for the line closest to the excavation bottom (line 8), which was approximately 65 kN. The steel rebar used in the nail has a diameter of 16 mm (Décourt et al., 2003) and a theoretical

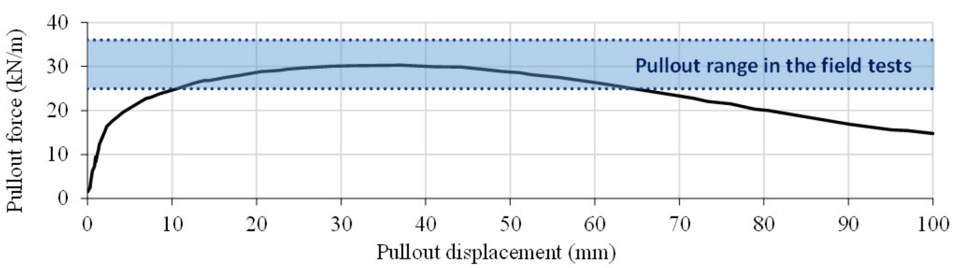

Figure 4. Pullout resistance behavior versus pullout displacement in FEM.

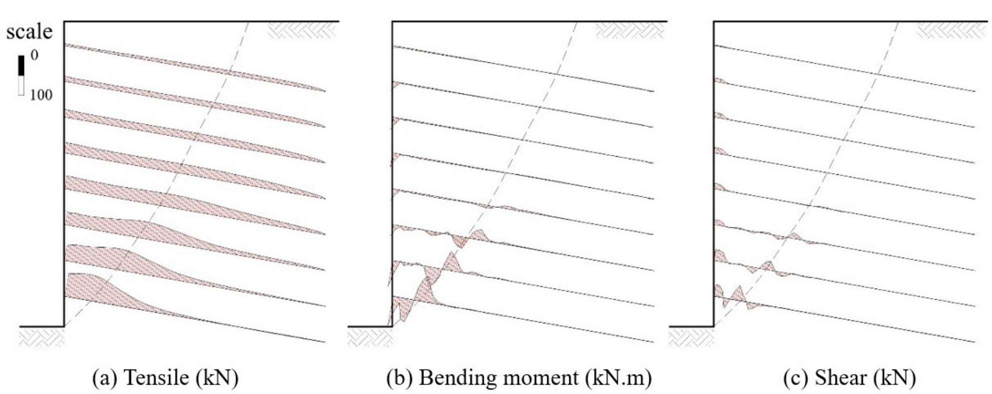

Figure 5. Tensile force (a), bending moment (b) and shear force (c) along nails length.

Table 2. Maximum and head tensile loads in the nails.

Nail row (top to bottom)	T_{max} (kN)	T_0 (kN)	T_0 / T_{max}
1	9.62	4.65	0.48
2	12.66	12.66	1.00
3	19.00	19.00	1.00
4	25.86	25.86	1.00
5	32.90	32.00	0.97
6	42.25	28.19	0.67
7	52.82	38.39	0.73
8	64.84	56.76	0.88

ultimate tensile strength of 157 kN. Based on the information provided in Table 2, the maximum tensile load in the nails throughout the excavation can be concluded to correspond to approximately 40% of the ultimate strength of the rebar. Additionally, the values shown in Table 2 indicate that the tensile loads in the nails range from 6% to 41% of the ultimate strength of the reinforcement, with an average value of 21%.

When analyzing the distribution of tensile loads along the nail length in Figure 5, a difference in behavior is observed between the lower and upper inclusions along the retaining wall depth. In the inclusions closer to the excavation bottom, the tensile forces are concentrated near the region where the maximum tensile load occurs. Conversely, in the reinforcements closer to the top, the tensile forces are more evenly distributed along the length of the nails. This difference in behavior can be attributed to two factors. Firstly, in the case of the upper nails, the magnitude of the tensile forces is lower. As a result, due to the rigidity of the steel rebar in the nail, the tensile force is more uniformly distributed along the entire length of the inclusion. This contrasts with the lower reinforcements, where the opposite condition occurs. Overall, the distribution of tensile loads along the nail length varies depending on the position of the inclusion, with a more concentrated distribution in the lower inclusions and a more uniform distribution in the upper inclusions. The line that connects the points of maximum nail tensile strength along the depth of the excavation intersects the surface at approximately 7.0 m from the face. This line exhibits a curvilinear shape, which is expected for a soil nailing retaining wall (Byrne et al., 1998). The relationship between the distance at which the maximum tensile line crosses the surface and the excavation height (H) is approximately 0.6H. This value is slightly higher than what is typically observed for soil nailing, but it could be attributed to the high cohesion of the excavated soil (Byrne et al., 1998; Clouterre, 1991).

In Figure 5, the highest values of bending moments acting in the nails are observed to also occur near the bottom of the excavation, corresponding to the highest tensile loads. The maximum bending moment is calculated to be 7.5 x 10^{-4} kN.m and occurs at the deepest inclusion. This magnitude is significantly lower than the maximum tensile load of 64.8 kN obtained for the same inclusion. This behavior indicates that, in the stabilization of the soil mass, the contribution of bending moments in the nails is only marginal compared to the tensile force. As a result, several methodologies disregard the bending moment in their calculation methods (Clouterre, 1991; Shen et al., 1981a; Stocker, 1979).

Similarly, the highest shear force values in Figure 5 are also observed near the bottom of the excavation, and this can be explained in a similar manner. Just like the bending moments, the magnitude of shear forces is reduced, even in the lowest nails, with values calculated up to 0.39 kN. When compared to the tensile loads, it can once again be concluded that shear forces contribute only marginally to the stabilization of the soil mass when using the soil nailing technique.

Figure 6 presents a comparison between the maximum nail load results from the FEA for the current study and those from other instrumented works in the U.S.A. These results are available in the FHWA-AS-96-069R report (Byrne et al., 1998). The FHWA report provides values of the maximum nail load, which are normalized by the coefficient of active earth pressure (K_a), soil specific weight (γ), excavation height (H), and spacing between the nails in the vertical (S_v) and horizontal (S_h) directions. The comparison includes data from eleven different soil nail works constructed and instrumented in the USA.

Figure 6 illustrates that the results of the maximum nail load, normalized values from the FEA of this study, fall within the range indicated for instrumented works in the U.S.A. (Byrne et al., 1998; Lazarte et al., 2015). However, it is observed that the results from the present study are located near the lower limit of the reported range. This can be attributed to the high apparent cohesion of the excavated clayey soil, which significantly reduces the horizontal stresses throughout the excavation. As a result, the lateral earth pressure and nail loads are reduced, and this cohesion effect is captured by the normalization of nail loads. Note that the chart used for comparison was prepared without considering the soil cohesion component, which was only marginal for the instrumented works, as described in the manual itself (Byrne et al., 1998).

Based on the FEM results, the analysis suggests a pattern for the maximum nail loads in relation to depth, as observed and discussed earlier. Specifically, when excluding the first point closest to the surface (which involves a horizontal spacing between nails half that of the rest of the retaining wall), the normalized maximum load in the nails remains relatively consistent with depth within the narrow range of 0.4 to 0.5. Notice that the last row produces a normalized maximum nail load that closely approaches the lower limit of 0.4, possibly due to the soil arch effect caused by the excavation bottom located approximately 1.0 m from that row.

4.4 State of stress in the soil

In excavation works and retaining walls, it is common practice to estimate and present the stress state in the soil at different depths using the coefficient of lateral earth pressure (K). When it comes to soil nailing excavations, the stress state can be evaluated by considering the maximum tensile load in the nails along the depth of the excavation (Clouterre, 1991). Figure 7 illustrates the values of parameter K as a function of

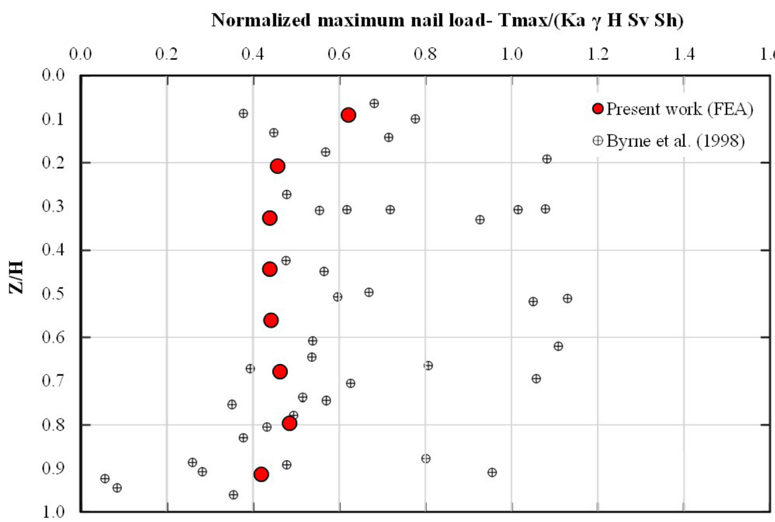

Figure 6. Comparison of the normalized maximum nail loads from the present work with data from instrumented works in the USA.

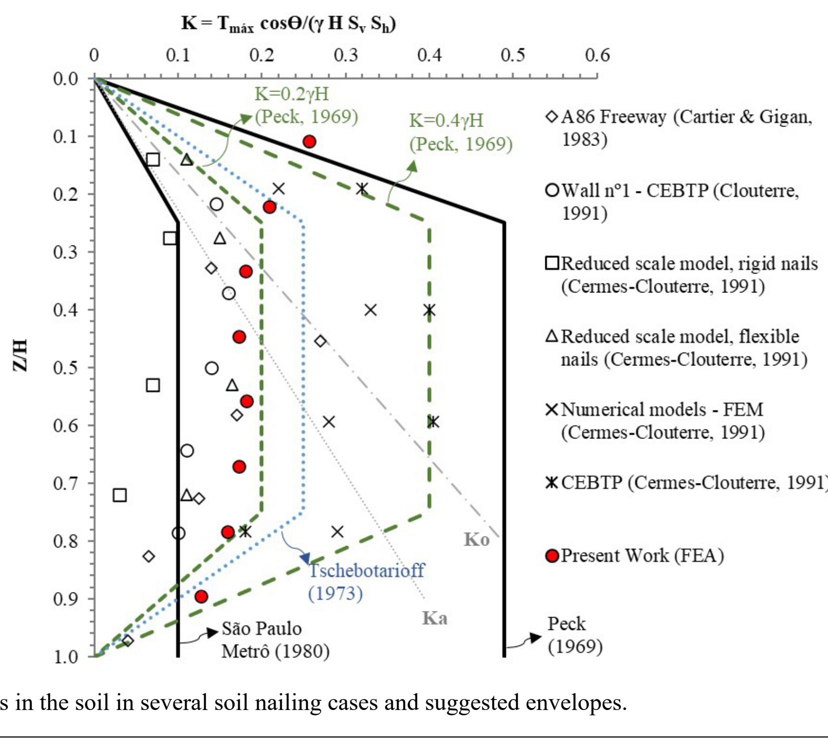

Figure 7. State of stress in the soil in several soil nailing cases and suggested envelopes.

the normalized depth (*z/H*) obtained from the FEA. The figure also includes the parameter *K* values reported in various cases in the literature (Cartier & Gigan, 1983; Clouterre, 1991) for comparison, representing the at rest and active states (K_0 and K_a lines), as well as suggested envelopes for different soil types (Peck, 1969; São Paulo Metro, 1980; Tschebotarioff, 1973).

Figure 7 demonstrates that the parameter *K* obtained from the FEA in this study falls within the range reported in the literature for several cases, including real structures, such as the A86 Freeway and Wall °1-CEBTP, as well as reduced scale models with flexible nails. The results from this study closely resemble those previously measured in these structures. Similarly to the mentioned cases, the parameter *K* in this study exhibits a consistent trend within a range of 0.1 to 0.2 throughout the depth of the excavation, with a slight decrease in value near the bottom of the excavation due to the soil arching effect. As described earlier, the first row is an exception and does not align with the rest of the excavation due to a change in the horizontal spacing between the nails.

Figure 7 illustrates that at the top of the excavation in the present study, similarly to the other cases shown in the figure, the stress state is very close to the at rest condition (K_0). This can be attributed to the presence of nails that restrict horizontal displacements at the top of the retaining wall, particularly when the horizontal spacing is smaller in the first row, as observed in the present case. Additionally, near the bottom of the excavation, the stress state is observed to be lower than in the active state condition, which can be attributed to the soil arching effect.

A comparison between the results of these various cases and certain envelopes proposed by different authors for braced excavations under different conditions also can be made from Figure 7. Most results from real cases (including the reduced-scale model with extensible reinforcements) closely align with the trapezoidal envelope proposed by Peck (1969) for stiff clays, with a value of $0.2\gamma H$. In fact, this envelope is even closer to the results from the present study than the suggestion provided in the São Paulo Metro Manual for braced excavations, which recommends a ratio of $0.1\gamma H$ for typical local soils (São Paulo Metro, 1980).

4.5 Nail tensile load at the head

Table 2 presents the tension load at the head (T_0) for each row of nails and its relationship with the maximum nail load (T_0/T_{max}) obtained from the FEA in the present study. Similarly to the maximum tensile force, the load at the head increases with depth. This behavior can be explained by the same factors discussed in section 4.3. The highest value calculated for the loads at the head was approximately 57 kN, which occurred in the row closest to the base of the excavation (line 8).

The T_0/T_{max} ratio throughout the height of the soil nailing retaining wall ranged from 0.5 to 1.0. In the first row, near the top, this ratio was at its lowest value due to the smaller horizontal spacing between the reinforcements. Up to approximately 60% of the excavation depth (up to line 5), the T_0/T_{max} ratio was observed to be very close to 1.0, and then decreased to a range between approximately 0.7 to 0.9 in the lower excavation portion. These values obtained from the FEM fall within the range typically described in the literature and recommended by manuals, which suggests a T_0/T_{max} ratio of 0.5 to 1.0 for spacing between nails close to 1.3 m (Byrne et al., 1998; Clouterre, 1991; Joshi & Asce, 2003; Lazarte et al., 2015).

Figure 8 presents a comparison between the results of tensile loads at the head from the FEA in our study and those from other instrumented works in the U.S.A., as

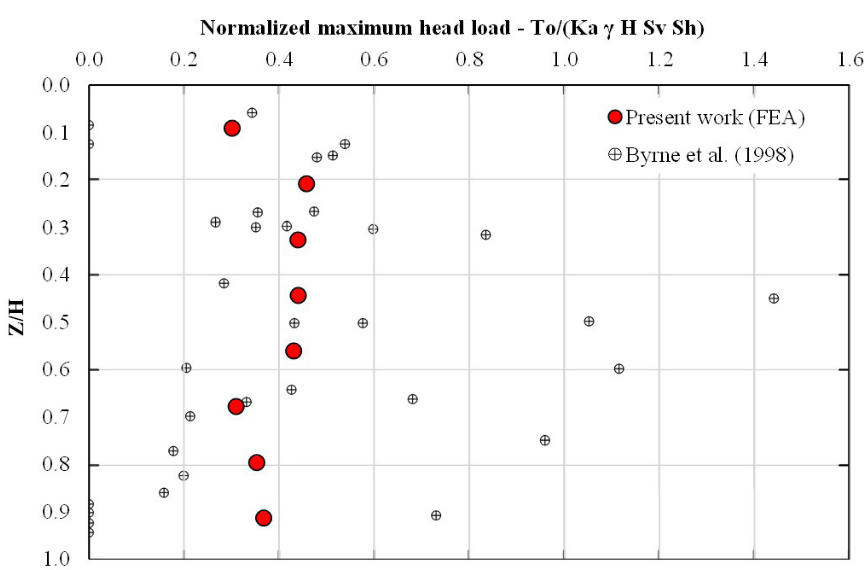

Figure 8. Comparison of the normalized nail loads at the head from the present work with data from instrumented works in the USA.

documented in the FHWA-AS-96-069R report (Byrne et al., 1998). Similarly to Figure 6, the head loads are once again normalized by the coefficient of active earth pressure (K_a), soil specific weight (γ), excavation height (H), and spacing between the nails in the vertical (S_v) and horizontal (S_h) directions. The comparison includes data from nine different soil nail works constructed and instrumented in the U.S.A.

Figure 8 illustrates that the results of the head load, normalized values obtained from FEA, fall within a range of 0.3 to 0.5. The normalized values tend to be higher in the upper half of the retaining wall, ranging between 0.4 and 0.5, and lower in the lower half, ranging between 0.3 and 0.4. This trend of higher normalized values at the top and lower values at the bottom is also reported by other authors (Byrne et al., 1998; Lazarte et al., 2015). As an exception, notice the first nail row, which, due to the smaller horizontal spacing between the reinforcements, resulted in a normalized maximum head load that deviates from the general behavior observed in the upper half of the excavation.

Figure 8 also allows concluding that the results of the head load, as obtained from the FEA, fall within the range of values reported for instrumented works in the U.S.A. In fact, as observed in this figure, the results from the present study are located close to the lower limit of the reported range, similarly to the findings for T_{max}. Two possible explanations can be considered for these results: i. the excavated clayey soil may have a high apparent cohesion, as previously explained; ii. the connection system between the nails and the shotcrete face may play a role. In the instrumented works in the U.S.A., a steel bearing plate (typically between 200 to 300 mm square and 15 to 20 mm thick) is used as the connection system. However, in this study, a different connection system was employed, which involves bending the end of the rebar (approximately 200 mm) in an "L" shape and tying it to the metal wire mesh of the shotcrete face. This connection system used in the present study is significantly less rigid than the one used in the instrumented works in the USA. Consequently, it can lead to lower loads at the head and on the shotcrete face.

5. Conclusion

This paper presented results, analyses, and discussion of an urban excavation supported by soil nailing in fine-grained soils, which were evaluated by FEA. A 3D FEM model was developed, incorporating two walls of the excavation retaining structure, with one wall being instrumented and used for the analyses in this study. Several field and laboratory soil investigations were conducted, interpreted and used in the FEA. The FEM model was calibrated using the instrumentation and monitoring data collected during the soil nailing construction. Several analyses were performed, including evaluation of horizontal displacements, nail pullout strength, nail tensile load, soil stress state, and tensile load at the head. Based on the results and discussion, the following conclusions can be drawn:

- In contrast to what is typically reported in the literature for fine-grained soils, the maximum displacements observed in this study were significantly lower than expected, reaching $\delta h/H = 0.06\%$. These maximum displacements occurred at approximately half of the excavation height.
- The nail pullout behavior observed in the FEA closely matched the results from field tests in this study. The skin friction values obtained from both the present work and FEA fell within the range recommended by various authors for clayey soils. The correlations between skin friction and the Standard Penetration Test yielded promising results, consistent with those obtained in the present work and FEA.
- The results from the FEM regarding the maximum nail tensile load (T_{max}) are as follows: (1) Higher values were observed at the bottom of the excavation; (2) The magnitude of these values was reduced, representing only about 5 to 40% of the ultimate strength of the nail rebar; (3) The line connecting the points of maximum loads along the height of the excavation intersects the surface at a distance from the face equal to $0.6H$; (4) This line has a curvilinear shape, which is expected for a soil nailing retaining walls; and (5) The normalized maximum tensile load values ranged from 0.4 to 0.5 and remained constant with depth. These values were lower than those observed in other instrumented works in non-cohesive soils.
- FEA revealed that the bending moments and shear forces in all nails were significantly reduced. This indicates that their contributions to this soil nailing structure are only marginal.
- The evaluation of the soil stress state using the FEM revealed that the region at the top of the excavation tends to have a state of stress similar to the at-rest condition. However, the region at the base of the excavation is in a state below the active condition, with K-values ranging from 0.1 to 0.2. The lower range of the envelope for braced excavations in stiff clays, as proposed by Peck (1969), provided the most accurate prediction for the FEM results in this study.
- The results from the loads at the head (T_0) are as follows: (1) The magnitudes of the loads at the head were low, similar to the maximum nail tensile loads; (2) The ratio T_0/T_{max} was close to 1.0 for the upper half of the excavation and ranged from 0.7 to 0.9 for the lower half of the retaining wall; and (3) The normalized load values ranged from approximately 0.3 to 0.5, which is lower than what has been observed in other instrumented works in non-cohesive soils.
- From this research results, it seems that if the fine-grained soil maintains its high apparent cohesion

throughout the structure lifespan, it can result in good performance by minimizing horizontal displacements and reducing the loads in the nails and at the head.

Acknowledgements

The authors would like to thank the Solotrat Company and P.E. Luciano Decourt for the valuable information provided.

Declaration of interest

The authors have no conflicts of interest to declare. All co-authors have observed and affirmed the contents of the paper and there is no financial interest to report.

Authors' contributions

Daniel Rocha Lanzieri: data curation, investigation, methodology, formal analysis. José Orlando Avesani Neto: conceptualization, supervision, validation, writing – original draft.

Data availability

The datasets generated analyzed in the course of the current study are available from the corresponding author upon request.

Declaration of use of generative artificial intelligence

This work was prepared without the assistance of Generative Artificial Intelligence (GenAI) tools.

List of symbols and abbreviations

c'	Soil apparent cohesion
d	Shotcrete thickness
q_s	Skin friction
w/c	Water-cement ratio
E	Young modulus
EA	Axial stiffness
EI	Bending stiffness
FEA	Finite Element Analysis
FEM	Finite Element Method
FHWA	Federal Highway Administration
G_0	Initial shear modulus
H	Excavation height
K	Coefficient of lateral earth pressure
K_a	Coefficient of active earth pressure
K_0	Coefficient of lateral earth pressure at rest
L	Nail lenght
$Nspt$	Number of blows in the standard penetration test
S_h	Nail horizontal spacing
S_v	Nail vertical spacing
T_{max}	Maximum tensile forces
T_0	Head tensile forces
γ	Unit weight
$\delta h/H$	Equivalent horizontal strain
υ	Poisson's ratio
ϕ'	Angle of internal friction
$\O$	Grouted diameter

References

Arêdes, A.C.N.B., Marques, E.A.G., & Oliveira, A.H.C. (2020). Pullout testing of soil nails in gneissic residual soil. *Soils and Rocks*, *43*(1), 85-96. http://doi.org/10.28927/SR.431085.

ASTM International. (2000). *ASTM Standard, D2487, 2000: Standard Practice for Classification of Soils for Engineering Purposes. Unified Soil Classification System*. ASTM International.

Babu, G., & Singh, V. (2010). Soil nails field pullout testing: evaluation and applications. *International Journal of Geotechnical Engineering*, *4*(1), 13-21. http://doi.org/10.3328/IJGE.2010.04.01.13-21.

Babu, G.L.S., Rao, R.S., & Dasaka, S.M. (2007). Stabilisation of vertical cut supporting a retaining wall using soil nailing: a case study. *Proceedings of the Institution of Civil Engineers - Ground Improvement*, *11*(3), 157-162. http://doi.org/10.1680/grim.2007.11.3.157.

Banthia, N., Trottier, J.-F., Beaupre, D., & Wood, D. (2011). Properties of steel fiber reinforced shotcrete. *Canadian Journal of Civil Engineering*, *21*(4), 564-575. https://doi.org/10.1139/l94-058.

Barbosa, M.G.T., de Assis, A.P., & da Cunha, R.P. (2022). An innovative post grouting technique for soil nails. *Geotechnical and Geological Engineering*, *40*(11), 5539-5546. http://doi.org/10.1007/s10706-022-02231-5.

Barbosa, M.G.T., Ferreira, L.R., de Souza, G.J.T., da Cunha, R.P., & Palmeira, E.M. (2023). 3D numerical analysis of soil nailing in sedimentary soil with vertical inclusions. *Soils and Rocks*, *46*(4), e2023005723. http://doi.org/10.28927/SR.2023.005723.

Bi, G., Liu, T., Wang, M., Xu, H., & Sun, Y. (2023). Creep behavior of soil nails in the high-PI clay. *Arabian Journal of Geosciences*, *16*, 310. https://doi.org/10.1007/S12517-023-11372-7.

Blondeau, F., & Ledeuil, E. (1984). Fouille clouée de grande profondeur (usine E.D.F. de Ferrières-sur-Ariège). *Revue Française de Géotechnique*, *29*, 35-42. http://doi.org/10.1051/geotech/1984029035.

Briaud, J.-L., & Lim, Y. (1997). Soil-nailed wall under piled bridge abutment: simulation and guidelines. *Journal of Geotechnical and Geoenvironmental Engineering*, *123*(11), 1043-1050. http://doi.org/10.1061/(ASCE)1090-0241(1997)123:11(1043).

Briaud, J.-L., Griffin, R., Yeung, A., Soto, A., Suroor, A., & Park, H. (1998a). *Long-term behavior of ground anchors and tieback walls*. Texas A & M Transportation Institute.

Briaud, J.-L., Powers III, W.F., & Weatherby, D.E. (1998b). Should grouted anchors have short tendon bond length?

Journal of Geotechnical and Geoenvironmental Engineering, *124*(2), 110-119. http://doi.org/10.1061/(ASCE)1090-0241(1998)124:2(110).

Bustamante, M., & Doix, B. (1985). Une methode pour le calcul des tirants et des micropieux injectes. *Bulletin de Liaison des Laboratoires des Ponts et Chaussées*, *140*, 75-92.

Byrne, R. J., Cotton, D., Porterfield, J., Wolschlag, C., & Ueblacker, G. (1998). *Soil manual for design and construction monitoring of soil nail wal* (No. FHWA-SA-96-069R). Federal Highway Administration Division.

Cartier, G., & Gigan, J.P. (1983). Experiments and observations on soil nailing structures. In *Proceedings of the 7th Conference of the ECSMFE* (pp. 473-476). Editora.

Clouterre. (1991). *Recommendations Clouterre. Project National Clouterre*. Presses de 1'ENPC.

Décourt, L., Zirlis, A., & Pitta, C. A. (2003). Design and behavior of excavations stabilized with soil nailing in Sao Paulo. In *Soil Nailing Workshop - Design, Execution, Instrumentation and Behavior* (pp. 57-104). ABMS.

Delmondes Filho, A. L., Cavalcante, E. H., Cardoso Júnior, C. R., & Cavalcanti Júnior, D. A. (2022). Study of the behavior of an instrumented soil nail wall in Salvador-Brazil. *Soils and Rocks*, *45*(4), e2022076221. http://dx.doi.org/10.28927/SR.2022.076221.

Ehrlich, M., & Silva, R.C. (2015). Behavior of a 31 m high excavation supported by anchoring and nailing in residual soil of gneiss. *Engineering Geology*, *191*, 48-60. http://doi.org/10.1016/j.enggeo.2015.01.028.

Fioravante, V., Jamiolkowski, M., & Lancellotta, R. (1994). An analysis of pressuremeter holding tests. *Geotechnique*, *44*(2), 227-238. http://doi.org/10.1680/geot.1994.44.2.227.

Gassler, G., & Gudehus, G. (1981). Soil nailing-some aspects of a new technique. In *Proceedings of the 10th International Conference on Soil Mechanics and Foundation Engineering* (pp. 665-670). ISSMGE.

Goyal, A., & Shrivastava, A.K. (2022). Analysis of conventional and helical soil nails using finite element method and limit equilibrium method. *Heliyon*, *8*(11), e11617. http://doi.org/10.1016/j.heliyon.2022.e11617.

Guilloux, A., & Schlosser, F. (1982). Soil nailing: practical applications. In *Symposium on Recent Developments in Ground Improvement Techniques* (pp. 389-397). Bangkok.

Guilloux, A., Notte, G., & Gonin, H. (1983). Experiences on retaining a structure by nailing in marine soils. In *Proceedings of Europan Conference on Soil Mechanics and Foundation Engineering* (Vol. 2, pp. 499-502). Helsinki.

Hogentogler, C.A., & Terzaghi, K. (1929). Interrelationship of load, road and subgrade. *Public Roads*, 10, 37-64.

Joshi, B., & Asce, M. (2003). Behavior of calculated nail head strength in soil-nailed structures. *Journal of Geotechnical and Geoenvironmental Engineering*, *129*(9), 819-828. http://doi.org/10.1061/(ASCE)1090-0241(2003)129:9(819).

Juran, I., & Elias, V. (1987). Soil nailed structures: analysis of case histories. In J. P. Welsh (Ed.), *A ten year update of soil improvement techniques, Geosynthetics for soil improvement* (ASCE Geotechnical Special Publication, No. 12, pp. 232-244). ASCE.

Kamath, A.C. (2016). *An experimental and numerical study on creep behavior of soil nail walls in high plasticity clays*. [Master's thesis]. Texas A & M University.

Lazarte, C. A., Robinson, H., Gómez, J. E., Baxter, A., Cadden, A., & Berg, R. (2015). *Geotechnical engineering circular No. 7 soil nail walls—Reference manual* (No. FHWA-NHI-14-007). Federal Highway Administration Division.

Look, B. (2007). *Handbook of geotechnical investigation and design tables*. Taylor & Francis Group. http://doi.org/10.1201/9780203946602.

Malmgren, L. (2007). Strength, ductility and stiffness of fibre-reinforced shotcrete. *Magazine of Concrete Research*, *59*(4), 287-296. http://doi.org/10.1680/macr.2007.59.4.287.

Massad, F. (2012). Shear strength and deformability of the sedimentary soils of São Paulo. In A. Negro, M. Namba, A. S. Dyminski, V. L. Sanches & A. C. M. Kormann (Eds.). *Twin cities - soils of the metropolitan regions of São Paulo and Curitiba* (pp. 109-135). Brazilian Association of Soil Mechanics and Geotechnical Engineering (ABMS).

Menkiti, C.O., & Long, M. (2008). Performance of soil nails in Dublin glacial till. *Canadian Geotechnical Journal*, *45*(12), 1685-1698. http://doi.org/10.1139/T08-084.

Mun, B., & Oh, J. (2017). Hybrid soil nail, tieback, and soldier pile wall – case history and numerical simulation. *International Journal of Geotechnical Engineering*, *11*(1), 1-9. http://doi.org/10.1080/19386362.2016.1177157.

Nicholson, P.J. (1986). In situ earth reinforcement at cumberland Gap, U.S. 25E. In *American Society of Civil Engineers and Pennsylvania Department of Transportation Joint Conference* (pp. 1-21). ASCE.

Oliaei, M., Norouzi, B., & Binesh, S.M. (2019). Evaluation of soil-nail pullout resistance using mesh-free method. *Computers and Geotechnics*, *116*, 103179. http://doi.org/10.1016/j.compgeo.2019.103179.

Oral, T., & Sheahan, T.C. (1998). The use of soil nails in soft clays. In *Design and Construction of Earth Retaining Systems* (pp. 26-40). ASCE.

Ortigão, J.A.R. (1997). Pullot tests in soil nailing structures. *Soils and Rocks*, *20*(1), 39-43.

Ortigão, J.A.R., Palmeira, E.M., & Zirlis, A.C. (1995). Experience with soil nailing in Brazil: 1970-1994. *Proceedings of the Institution of Civil Engineers - Geotechnical Engineering*, *113*(2), 93-106. http://doi.org/10.1680/igeng.1995.27589.

Ortigão, J.A.R., Palmeira, E.M., & Zirlis, A.C. (1997). Optimised design for soil nailed walls. In *Proceedings of the 3rd Internacional Conference on Ground Improvement Geosystems* (pp. 368-374). Thomas Telford; ASCE.

Ostermayer, H. (1975). PAPER 18 Construction, carrying behaviour and creep characteristics of ground anchors. In *Diaphragm Walls & Anchorages* (pp. 141-151). The Institution of Civil Engineers.

Papagiannakis, A.T., Diaz, M., & Bin-Shafique, S. (2016). Numerical analysis of a soil nail wall system in expansive clays. In *Transportation Research Board 95th Annual Meeting*. Washington. Retrieved in October 25, 2023, from https://trid.trb.org/view/1393038

Peck, R.B. (1969). Deep excavations and tunneling in soft ground. In *Proceedings of the 7th International Conference on Soil Mechanics and Foundation Engineering* (pp. 225-290). ISSMGE.

Plumelle, C. (1986). *Special lecture for the French National Committee of Soil Mechanics*. ISSMGE.

Poon, B., Mitchell, P.W., Oko-Oboh, D., & Pham, M. (2019). Design and construction of soil nail wall on the basis of unsaturated soil mechanics. In *Proceedings of the 13th Australia New Zealand Conference on Geomechanics* (pp. 1023-1028). Western Australia. Retrieved in October 25, 2023, from https://trid.trb.org/view/1647570

Portelinha, F.H.M., Goulart, J.M.H., & Avesani Neto, J.O. (2023). Influence of heterogeneous arrangements of reinforcements' length and stiffness on the deformation of instrumented geosynthetic-reinforced retaining walls constructed with sustainable locally available backfill soils. *Sustainability (Switzerland)*, *15*(10), 8183. http://doi.org/10.3390/su15108183.

Porto, T.B., Torres, A.C.A., & Gomes, R.C. (2017). Behavior of reinjectable and prestressed anchors in soil masses: construction case study in Congonhas - Brazil. *Soils and Rocks*, *40*(2), 177-186. http://doi.org/10.28927/SR.402177.

Pradhan, B., Tham, L.G., Yue, Z.Q., Junaideen, S.M., & Lee, C.F. (2006). Soil–nail pullout interaction in loose fill materials. *International Journal of Geomechanics*, *6*(4), 238-247. http://doi.org/10.1061/(ASCE)1532-3641(2006)6:4(238).

Sanchez, M., Briaud, J.-L., Hurlebaus, S., Kharanaghi, M.M., & Bi, G. (2017). *Creep behavior of soil nail walls in high plasticity index (PI) soils: technical report*. T. A. T. Institute. https://doi.org/10.21949/1503647.

Santos, J., & Correia, A. (2001). Reference threshold shear strain of soil. Its application to obtain an unique strain-dependent shear modulus curve for soil. In *Proceedings of the 15th International Conference on Soil Mechanics and Geotechnical Engineering* (pp. 267-270). ISSMGE.

São Paulo Metro. (1980). *NC-03: Technical standards* (Vol. 2). Sao Paulo Metropolitan Company.

Shen, C.K., DeNatale, J.S., Kulchin, L., Romstad, K.M., & Bang, S. (1981a). Field measurements of an earth support system. *Journal of the Geotechnical Engineering Division*, *107*(12), 1625-1642. http://doi.org/10.1061/AJGEB6.0001217.

Shen, C.K., Herrmann, L.R., & Bang, S. (1981b). Ground movement analysis of earth support system. *Journal of the Geotechnical Engineering Division*, *107*(12), 1609-1624. http://doi.org/10.1061/AJGEB6.0001216.

Silva, D. P. e. (2009). *Analysis of different soil nailing executive methods from pullout tests performed in field and laboratory* [Doctoral thesis, São Carlos School of Engineering, University of São Paulo]. University of São Paulo (in Portuguese). https://doi.org/10.11606/T.18.2009.tde-22032010-102032.

Singh, V.P., & Sivakumar Babu, G.L. (2010). 2D numerical simulations of soil nail walls. *Geotechnical and Geological Engineering*, *28*(4), 299-309. http://doi.org/10.1007/s10706-009-9292-x.

Solotrat. (2017). 14 cases of soil nail in Brazil. In *Seminar presented at the Polytechnic School of the University of São Paulo (EPUSP)*. USP. In Portuguese.

Stocker, M. F. (1979). Soil nailing. In *International Conference on Soil Reinforcement* (pp. 469-474). ARRB.

Su, L.-J., Chan, T.C.F., Yin, J.-H., Shiu, Y.K., & Chiu, S.L. (2008). Influence of overburden pressure on soil–nail pullout resistance in a compacted fill. *Journal of Geotechnical and Geoenvironmental Engineering*, *134*(9), 1339-1347. http://doi.org/10.1061/(ASCE)1090-0241(2008)134:9(1339).

Su, L.-J., Yin, J.-H., & Zhou, W.-H. (2010). Influences of overburden pressure and soil dilation on soil nail pull-out resistance. *Computers and Geotechnics*, *37*(4), 555-564. http://doi.org/10.1016/j.compgeo.2010.03.004.

Suksawang, N., Wtaife, S., & Alsabbagh, A. (2018). Evaluation of elastic modulus of fiber-reinforced concrete. *ACI Materials Journal*, *115*(2), 239-249. http://doi.org/10.14359/51701920.

Taib, S.N.L., & Craig, W.H. (2006). Modeling construction and failure of soil nailed structures in clay. In *Proceedings of the Sixth International Conference on Physical Modelling in Geotechnics* (pp. 577-583). CRC Press.

Tschebotarioff, G. (1973). *Foundations, retaining and earth structures: the art of design and construction and its scientific basis in soil mechanics*. McGraw-Hill Education.

Turner, J.P., & Jensen, W.G. (2005). Landslide stabilization using soil nail and mechanically stabilized earth walls: case Study. *Journal of Geotechnical and Geoenvironmental Engineering*, *131*(2), 141-150. http://doi.org/10.1061/(ASCE)1090-0241(2005)131:2(141).

Yadegari, S., Yazdandoust, M., & Momeniyan, M. (2023). Performance of helical soil-nailed walls under bridge abutment. *Transportation Geotechnics*, *38*, 100788. http://doi.org/10.1016/j.trgeo.2022.100788.

Ye, X., Wang, S., Wang, Q., Sloan, S.W., & Sheng, D. (2017). Numerical and experimental studies of the mechanical behaviour for compaction grouted soil nails in sandy soil. *Computers and Geotechnics*, *90*, 202-214. http://doi.org/10.1016/j.compgeo.2017.06.011.

Yuan, J., Lin, P., Huang, R., & Que, Y. (2019). Statistical evaluation and calibration of two methods for predicting nail loads of soil nail walls in China. *Computers and Geotechnics*, *108*, 269-279. http://doi.org/10.1016/j.compgeo.2018.12.028.

Zhou, Y., Xu, K., Tang, X., & Tham, L.G. (2013). Three-dimensional modeling of spatial reinforcement of soil nails in a field slope under surcharge loads. *Journal of Applied Mathematics*, *2013*(1), 926097. http://doi.org/10.1155/2013/926097.

Zhu, H.-H., Yin, J.-H., Yeung, A.T., & Jin, W. (2010). Field pullout testing and performance evaluation of GFRP soil nails. *Journal of Geotechnical and Geoenvironmental Engineering*, *137*(7), 633-642. http://doi.org/10.1061/(ASCE)GT.1943-5606.0000457.

Zolqadr, E., Yasrobi, S.S., & Norouz Olyaei, M. (2016). Analysis of soil nail walls performance - case study. *Geomechanics and Geoengineering*, *11*(1), 1-12. http://doi.org/10.1080/17486025.2015.1006263.